arXiv:1105.0114v1 [astro-ph.CO] 30 Apr 2011

CAUSTIC CROSSING EVENTS AND SOURCE MODELS IN GRAVITATIONAL LENS SYSTEMS

A.N. ALEXANDROV, V.M. SLIUSAR, V.I. ZHDANOV

Taras Shevchenko National University of Kyiv
(2, Academician Glushkov Prosp., Kyiv 03022, Ukraine; e-mail: alex@observ.univ.kiev.ua; vitaliy.slyusar@gmail.com; zhdanov@observ.univ.kiev.ua)

PACS 98.62.Sb
©2011

High amplification events (HAEs) are common phenomena in extragalactic gravitational lens systems (GLSs), where the multiple images of a distant quasar are observed through a foreground galaxy. There is a considerable brightness magnification in one of the quasar images during HAE. Grieger, Kayser, and Refsdal (1988) proposed to use HAEs to study the central regions of quasars in GLSs. In this paper, we consider some problems concerning the identification of different source types on the basis of the HAE observations. We compare the results of light curve simulations to estimate a feasibility to distinguish different source models in GLSs. Analytic approximation methods yielding solutions of the lens equation in a vicinity of fold caustic crossing events are presented. The results are used to obtain amplification factors, which the higher-order corrections for the Gaussian, power-law, and limb-darkening models of a source take into account.

1. Introduction

Gravitational lens systems can be viewed as natural telescopes that provide a valuable information about remote objects. In an extragalactic gravitational lens system (GLS), a distant quasar is observed through a foreground galaxy. The gravitational field of the galaxy can bend light rays from the source sufficiently so that there are multiple light rays that reach an observer. The observer sees an image in the direction of each ray, so that the source appears multiply imaged.

Light rays from a quasar pass through the lensing galaxy in different regions. Local variations of gravitational fields in these regions, which are mainly due to a relative motion of the lensing galaxy and the source, lead to considerable brightness variations in each image (gravitational microlensing), which can be detected even by modest telescopes. The typical time scales of these microlensing processes may vary from weeks to months. A comparison of the independent brightness variations in different images provides a valuable information about the lensing galaxy and about the source structure [1, 2]. One of the most important applications of the microlensing concerns a unique possibility to study a fine structure of the central quasar region that cannot be resolved in another way with modern observational techniques. This is important because the quasars in GLSs have high redshifts. Therefore, when studying the quasars, we learn something about a corresponding early epoch.

HAEs – considerable brightness magnifications in one of the images of a quasar – are common phenomena in extragalactic GLSs. Grieger, Kayser and Refsdal [3] proposed to use HAEs to study the central regions of the quasars in GLSs. Typically corresponding variations of the brightness in a neighborhood of the HAE can be approximately described by a formula containing a few fitting parameters. This makes it possible to estimate some GLS parameters, in particular, the source size [3]. For example, in case of the well-known GLS Q2237+0305 "Einstein Cross" [4], several HAEs were observed [5–7], and the estimates of the source size have been obtained for different source models [8–14]. Almost all HAEs in the Q2237+0305 GLS are attributed to the intersection of a fold caustic in the source plane (see, e.g., [15]). In view of the increasing accuracy of photometric observations, a possibility to distinguish different source models is also discussed (see, e.g., [16, 17]).

Here, we study some problems dealing mainly with the investigation of the source structure in an extragalactic GLS using the light curves of the source images. We discuss the results of simulations of light curves for different

microlensed source models and present some analytic approximations yielding solutions of the lens equation in a vicinity of the fold caustic crossing events. The results are used to obtain amplification factors for some source models that take the "post-linear" corrections into account.

Note that, in reality, we have, indeed, a unique light curve for each image of the quasar in a GLS. The high amplification events are not too frequent, and it may take a considerable time to accumulate a sufficient statistics and even to wait a repetition of the HAE. Thus, the main attention is paid to the determination of source properties from a single light curve compared with the light curves of the other images. On the other hand, since the work by Kochanek [18] followed by a number of works [15, 17, 19–23], numerous statistical methods have been developed to process complete light curves. These methods treat the whole available light curves from all the images, not only HAEs. There is an enormous number of the degrees of freedom which prohibit the simultaneous determination of *all* the parameters of a GLS (microlens positions, their masses, and the source parameters). But the observational data restrict possible realizations of the microlens masses and the positions, so one may estimate the conditional probability of certain parameter values. Such approach is very attractive because it allows one to use the whole aggregate of observational data on image light curves. However, this involves a large number of realizations of the microlensing field and, respectively, a considerable computer time.

On the other hand, the source structure manifests itself only in HAEs; far from the caustic, the source looks like a point one, and all the information about its structure is lost. If we restrict ourselves to a HAE neighborhood, then we use the most general model concerning a microlensing field described by a small collection of the Taylor expansion coefficients in the lens mapping.

The structure of this paper is as follows. Section 2 contains some basics of the gravitational lensing, a short review of the problems concerning the determination of a source model from HAE observations, and a list of typical models. In Section 3, we present the results of simulations for these source models, in particular, the differences of light curves. In Section 4, we outline approximation methods to investigate solutions of the lens equation used to derive the amplification coefficient of a point source. The result is used to obtain amplifications of an extended source near the fold caustic for some source models. Section 6 contains the discussion of the results.

2. General Relations and Notations

2.1. The lens equation

First, we recall some general notions concerning the gravitational lensing that can be found, e.g., in book [1]. The normalized lens equation has the form

$$\mathbf{y} = \mathbf{x} - \nabla\Phi\left(\mathbf{x}\right), \tag{1}$$

where $\Phi\left(\mathbf{x}\right)$ is the lens potential. This equation relates every point $\mathbf{x} = (x_1, x_2)$ of the image plane to the point $\mathbf{y} = (y_1, y_2)$ of the source plane. In the general case, there are several solutions $\mathbf{X}_{(i)}\left(\mathbf{y}\right)$ of the lens equation (1) that represent images of one point source at $\mathbf{y}$; we denote the solution number by the index in parentheses.

If there is no continuous matter on the line of sight, the potential must be a harmonic function: $\Delta\Phi = 0$. Below, we assume that this condition is fulfilled in a neighborhood of the critical point. We note, however, that if the continuous matter density is supposedly constant during a HAE, this can be taken into account by a suitable renormalization of the variables.

The amplification of a separate image of the point source is

$$K_{(i)}\left(\mathbf{y}\right) = 1/\left|J\left(\mathbf{X}_{(i)}\left(\mathbf{y}\right)\right)\right|, \tag{2}$$

where $J\left(\mathbf{x}\right) \equiv \left|D\left(\mathbf{y}\right)/D\left(\mathbf{x}\right)\right|$ is the Jacobian of the lens mapping. In the microlensing processes, microimages cannot be observed separately; therefore, we need the total amplification that is a sum of the amplification factors of all the images.

The critical curves of the lens mapping (1) are determined by the equation $J\left(\mathbf{x}\right) = 0$ and are mapped onto the caustic in the source plane. The stable critical points of a two-dimensional mapping can be folds and cusps only, the folds being more probable in a HAE. In this paper, we confine ourselves to the consideration of a fold caustic. When the point source approaches the fold caustic from its convex side, two of its images approach the critical curve, and their amplification tends to infinity. They disappear when the source crosses the caustic. These two images are called critical.

2.2. Problems

Let $I(\mathbf{y})$ be the initial surface brightness distribution of an extended source. If the source center is located at the point $\mathbf{Y} = (Y_1, Y_2)$ in the source plane, then the total microlensed flux from the source is

$$F(\mathbf{Y}) = \iint I(\mathbf{y}(\mathbf{x}) - \mathbf{Y})\, dx_1 dx_2, \tag{3}$$

$\mathbf{x} = (x_1, x_2)$. The result of using Eq. (3) is obviously equivalent to the result of the well-known ray-tracing method [1] (when the pixel sizes tend to zero).

An equivalent representation of this formula is

$$F(\mathbf{Y}) = \iint K(\mathbf{y}) I(\mathbf{y} - \mathbf{Y})\, dy_1 dy_2, \qquad (4)$$

where the point source amplification $K(\mathbf{y}) = \sum\limits_i K_i(\mathbf{y})$ is the sum of amplifications of all the images.

Near the caustic, one can approximate $K(\mathbf{y}) = K_0 + K_{\rm cr}(\mathbf{y})$, where K_0 is the amplification of all noncritical images that is supposed to be constant during HAE, and $K_{\rm cr}$ is the amplification of the critical images. Due to a relative motion of the lensing galaxy and the source (quasar), the flux is a function of time representing the light curve of some quasar image in the GLS. In the lensing galaxy rest frame, the quasar motion may be considered as a straight-line motion with a sufficient accuracy. Here, we are mostly interested in the caustic crossing events when the quasar intersects the caustic in the source plane leading to a considerable enhancement of the image brightness. The light curve yields information about the source structure and about the gravitational field of the lensing galaxy. Particularly, the form of a light curve near a HAE depends on the function $I(\mathbf{y})$, and the question is whether it is possible to use this dependence in order to identify this function.

To illustrate the typical problems arising in the conventional treatment of a HAE, we consider an approximate relation for the amplification coefficient $K_{\rm cr}(\mathbf{y})$ of a point source located at the point $\mathbf{y} = (y_1, y_2)$ of the source plane which is located near the fold. In the appropriate coordinate system, the amplification of a point source can be approximated as $K_{\rm cr}(y_1, y_2) = A_0(y_2)^{-1/2}\Theta(y_2)$ [1], where y_2 is the distance between the point source and the caustic, and $\Theta(y_2)$ is the Heaviside step function. The observed radiation flux from the extended source image during the HAE is then obtained from Eq.(4) yielding an integral equation for the one-dimensional luminosity profile $f(y_2) = \int I(y_1, y_2) dy_1$:

$$F(t) = C_1 + A_0 \int \Theta(y_2)(y_2)^{-1/2} f(y_2 - Y_2(t)) dy_2, \qquad (5)$$

$\mathbf{Y}(t) = (Y_1(t), Y_2(t))$ is the source center trajectory which can be written as a linear function of time; $F(t)$ is known from observations, C_1 describes a contribution of noncritical images and can be considered to be constant during the HAE. Thus, we have an equation for $f(y)$.

The main problems concerning with this equation are as follows.

(i) Equation (5) gives us nothing about the whole function $I(y_1, y_2)$ we are interested in, unless some suppositions about the form of the source are made, e.g., the supposition about circular symmetry. Also, even for known $F(t)$ and $Y_2(t)$, Eq. (5) presents a kind of the ill-posed mathematical problems: small variations of input data can lead to a considerable change of the solution. A standard way to relax this difficulty involves additional restrictions on $f(y)$ and/or the use of some explicit models for the brightness distribution $I(\mathbf{y})$ containing a small number of free parameters. Some of these models are considered below in the next subsection.

(ii) It is clear that a real brightness profile of the central quasar region is quite different from the simplified brightness distributions of the following section that can be considered rather as some reference models. However, in view of the present-day accuracy of observations, sometimes it can be difficult to distinguish even these simple source models using a HAE. For example, the authors of [17] argue that the light curves from a accretion disk can be well fitted with any brightness profile (Gaussian, uniform, *etc.*) of an appropriate source size. On the other hand, a number of authors [8–10, 15–19, 23] discussed the delicate questions concerning the determination a fine quasar structure from HAEs. For example, the authors of [16] wrote that the GLITP data [5] on Q2237+0305 admit only accretion disc models (see also [15, 19]). Obviously, the presence of an accretion disk in the central region of a quasar is beyond any doubts, as well as the fact that the real quasar core can be quite different from its simplified models in question. The question is how to prove *a posteriori* the existence of the accretion disk on a basis of available observational data.

One must also have in mind that, without using an additional information (besides HAEs), we cannot determine even the source size, because we do not know the value and the direction of the source velocity with respect to the caustic. Also, different ellipticities and orientations of the source may lead to different forms of the light curves during a HAE.

(iii) The kernel $K_{\rm cr}$ of the integral equation (5) is a result of the so-called linear caustic approximation of the lens equation. This will work correctly only in the case where the source size is much smaller than the caustic curvature radius. Below, we consider corrections to $K_{\rm cr}$ that arise in the post-linear approximation. However, these approximations also require the source to be sufficiently small. This requirement can be violated in case of a complicated caustic network or in the presence of a population of small microlenses (cf. planetary masses).

2.3. The extended source models

Below, we list the simplest most commonly used brightness distributions of the source in a GLS; without loss of generality, they are chosen to be normalized to 1:

$$\iint I(\mathbf{y})\, dy_1 dy_2 = 1.$$

To compare different models of brightness distribution, we have to use the same parameter that characterizes the size of an object. The most general is the r.m.s. size $R_{\rm rms}$:

$$R^2_{\rm rms} = \iint \mathbf{y}^2 I(\mathbf{y})\, dy_1 dy_2. \tag{6}$$

For a slowly decreasing brightness profile (e.g., $I(\mathbf{y}) \sim |\mathbf{y}|^{-\alpha}$, $\alpha \le 4$) the r.m.s. size diverges. In the case of the circularly symmetric sources, the half-brightness radius $R_{1/2}$ is also widely used; it is defined by the relation

$$2\pi \int\limits_0^{R_{1/2}} I(r) r\, {\rm d}r = \pi \int\limits_0^{\infty} I(r) r\, {\rm d}r. \tag{7}$$

In the case of the Gaussian source model,

$$I_G(r) = \frac{1}{\pi R^2} \exp\left[-\left(\frac{r}{R}\right)^2 \right], \tag{8}$$

where $R = R_{\rm rms}$, $R_{1/2} = R\sqrt{\ln(2)}$, and R stands for a size parameter.

The limb-darkening (LD) model (see, e.g., [24]) yields

$$I_{\rm LD}(r) = \frac{q+1}{\pi R^2}\, \Xi(r/R; q), \tag{9}$$

where

$$\Xi(\xi; q) = \Theta(1-\xi^2)(1-\xi^2)^q,$$

and $R^2 = (q+2)\, R^2_{\rm rms}$. Here, we assume $q > 0$. The half-brightness radius is $R_{1/2} = R\sqrt{1-(1/2)^{1/(q+1)}}$.

Models (9) and (8) describe a class of compact sources with a fast decrease in the brightness. On the contrary, the power-law models [9, 10] describe a slower decrease at large r:

$$I_{\rm PL}(r) = \frac{p-1}{\pi R^2} \left[1 + r^2/R^2\right]^{-p}, \tag{10}$$

where $p > 1$ is the exponent, and R is related to the r.m.s. radius $R_{\rm rms}$ as $R^2 = (p-2)\, R^2_{\rm rms}$. Model (10) is an alternative to (9). The half-brightness radius of the source within this model is $R_{1/2} = R\sqrt{2^{1/(p-1)} - 1}$. For fixed $R_{\rm rms}$ and $p \to \infty$, the brightness distribution (10) tends to the Gaussian one. For small p, we have a "long-range" distribution; $R_{\rm rms}$ diverges for $p \le 2$.

Linear combinations of different distributions with different parameters yield rather a wide class of symmetric source models.

A more complicated profile is presented by the Shakura–Sunyaev model (AD) of accretion disk [25]

$$I_{\rm AD}(r) = \frac{3R\theta(r-R)}{2\pi r^3} \left[1 - \sqrt{\frac{r}{R}}\right]. \tag{11}$$

For the AD model, the half-brightness radius is $R_{1/2} = 4R$, $R_{\rm rms} = \infty$

Another model [18, 25] (AD1) can be defined as

$$I_{\rm AD1}(r) = \frac{C_{\rm AD1}}{R^2} \left[\exp(\rho^{3/4}) - 1\right]^{-1}, \quad \rho = r/R, \tag{12}$$

$$C_{\rm AD1} = 3(8\pi\Gamma(8/3)\zeta(8/3))^{-1} \approx 0.06,$$

$\zeta(x)$ is the Riemann zeta function, $\Gamma(x)$ is the Gamma function, and

$$R^2_{\rm rms} = R^2 \frac{\Gamma(16/3)\zeta(16/3)}{\Gamma(8/3)\zeta(8/3)} \approx 21.4 R^2.$$

It is also interesting to study a superposition of the LD and AD models (LA), where the accretion disk has a boundary

$$I_{\rm LA}(r) = \frac{C(q)\Xi(\rho; q)}{R^2 \left[\exp(\rho^{3/4}) - 1\right]^{-1}}, \quad \rho = r/R, \tag{13}$$

where $C(q)$ is a normalizing coefficient; $C(1) = 0.42$, $C(2) = 0.54$, $C(3) = 0.64$.

3. Simulations of Light Curves

3.1. Equations of microlensing

In the case without continuous matter on the line of sight, the lens equation takes the form

$$\mathbf{y} = \mathbf{x} - R^2_{\rm E} \sum_{i=1}^{N} \frac{\mathbf{x} - \mathbf{x}_i}{|\mathbf{x} - \mathbf{x}_i|^2}, \tag{14}$$

where $\mathbf{x}_i$ are positions of the microlenses in the lens plane, and $R_{\rm E}$ is the radius of the Einstein ring for one microlens which is assumed to be the same, $R_{\rm E} = 1$, for all microlenses.

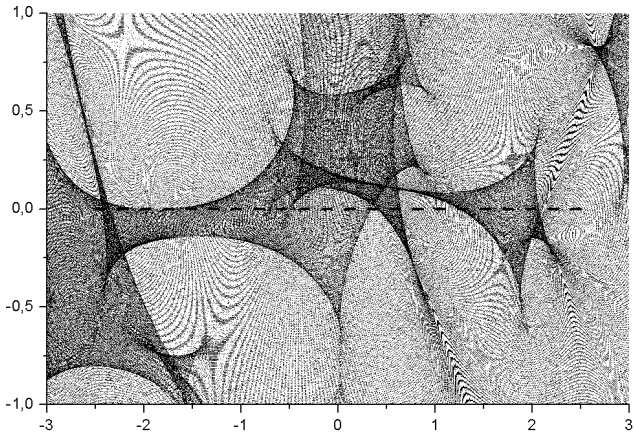


Fig. 1. Magnification pattern with the trajectory of the source in the source plane (coordinates are measured in $R_{\rm E}$ units). The source moves from left to right along the straight line with uniform speed

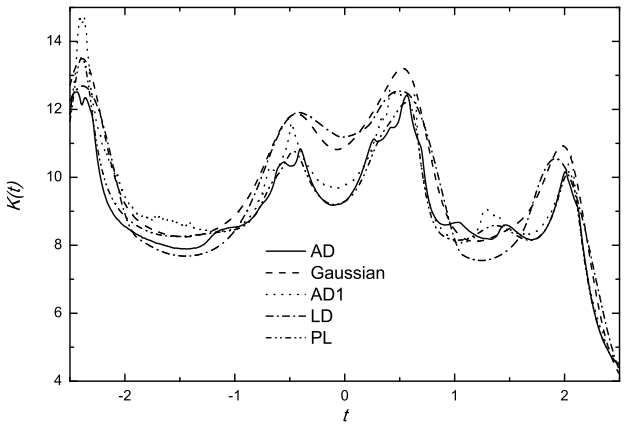


Fig. 2. "Light curves": the amplification as a function of time for different source models that correspond to the magnification pattern in Fig. 1

Here, we present the results of straightforward calculations of the microlensed flux (3) to obtain the light curves for different realizations of the microlens positions. All calculations were performed for the microlensing optical depth $\sigma = 0.3$. The total number of microlenses was 1470.

The microlens positions were chosen in a random way with uniform distribution over the field. The trajectory length has been taken so as to provide the caustic crossings. The size of the microlens field was chosen large enough to avoid boundary effects.

3.2. Light curves

The form of the light curve of the microlensed source in caustic crossing events depends on details of the source structure. However, the point is to determine the most relevant source model with regard for this form. In this work, we compare the light curves within the Gaussian, PL, LD, AD, and AD1 source models. The simulations were performed for the set of 100 realizations of a microlensing field with the optical depth $\sigma = 0.3$ corresponding to parameters of Q2237+0305 [26–29]. All models have the same half-brightness radius $R_{1/2}$. The calculations were performed for the same microlenses fields. The source speed is $V = 1$, so we can identify the source position as a function of time t. All the microlenses are static. The typical magnification pattern is shown in Fig. 1.

T a b l e 1. Parameters of simulation

Parameter	Value
Number of pixels	1.23×10^6
Pixel size	0.01 $R_{\rm E}$
Source trajectory length	2 $R_{\rm E}$; 5 $R_{\rm E}$
Radius of field	70 $R_{\rm E}$
Microlensing optical depth (σ)	0.3
Source speed (V)	1
Time discretization (δt)	0.01 $R_{\rm E}/V$

First, we present the results of simulations with the same half-brightness radius $R_{1/2} = 0.21$; the power-law exponent was $p = 3/2$ for the "long range" PL model; the AD model also corresponds to this class of the power-law asymptotic dependence with $p = 3/2$). For LD and LA models, we have chosen $q = 1$ throughout the paper. From the "light curves" in Fig. 2, we observe a significant difference between the compact (LD and Gaussian) and "long-range" models. The long-range character of the latter reveals itself even at considerable distances from the caustic, where we expect that the brightness of all sources must have the same behavior as that of a point source. The differences between these two groups of models are essentially larger than the differences within each group (e.g., between the Gaussian and LD models). This conclusion is confirmed by the results of statistical considerations over 100 realizations shown in Table 2 for the half-brightness radius $R_{1/2} = 0.21$ as an example.

To compare different models i and j, we used the relative difference

$$\eta = 2 \max_t \left(\frac{|K_i(t) - K_j(t)|}{K_i(t) + K_j(t)} \right), \qquad (15)$$

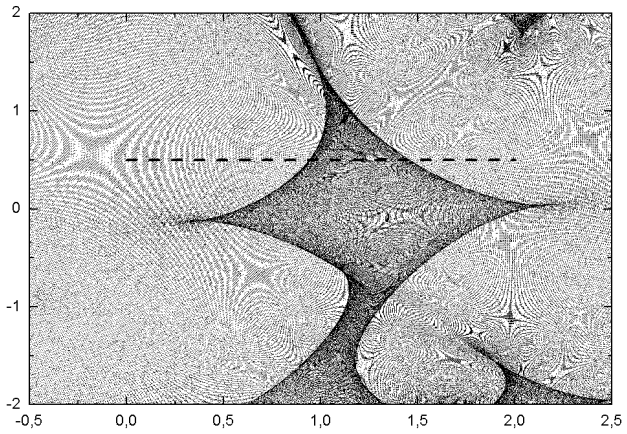


Fig. 3. Magnification pattern with simple caustic crossing events

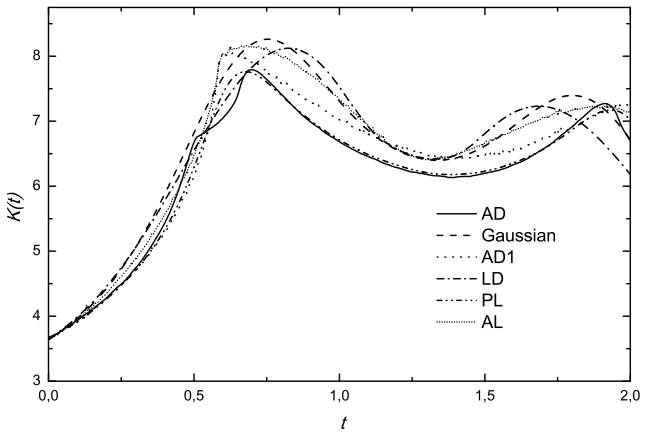


Fig. 4. Light curves (magnification curves) for different models of source brightness profile that correspond to the magnification pattern of Fig. 3

where $K_i(t)$ is the amplification for the i-th model along the trajectory of source's linear movement.

These results can depend on a complexity of the caustic involved into our consideration (i.e., there can be parts of the fold caustic close to the cusp points, or there can be dense aggregations of caustics). From many-year observations of the light curves of such GLS as Q2237+030, one can rule out such complex cases. Therefore, we considered some modification of our statistical consideration with rather simple fold caustic crossings. However, the numerical results of this modification with simple caustic crossing events (such as in Fig. 3,4 as an example) appeared to be nearly the same as those of Table 2. As an example, Table 3 shows the results of simulations analogous to those in Table 2 with the r.m.s. radius $R_{\rm rms} = 0.21$; here, we excluded the models with $R_{\rm rms} = \infty$ (here, $p = 3$ for the PL model). The larger error is due to a smaller number of realizations with the "simple" caustic.

T a b l e 2. Relative difference between models in HAE

i-th model	j-th model	η
AD	Gaussian	0.074 ± 0.0012
AD	AD1	0.085 ± 0.002
AD	LD	0.091 ± 0.002
AD	PL	0.038 ± 0.001
Gaussian	AD1	0.073 ± 0.0017
Gaussian	LD	0.042 ± 0.001
Gaussian	PL	0.073 ± 0.0013
AD1	LD	0.094 ± 0.002
AD1	PL	0.052 ± 0.0012
LD	PL	0.090 ± 0.002

3.3. Gaussian fittings of the accretion disk and limb darkening models

The above results concern with a comparison of different models *with the same* $R_{1/2}$ or $R_{\rm rms}$. However, in reality, we do not know the source model to fit, and one may ask why a light curve is not fitted within a different model. Therefore, one must verify whether we can replace one model with a different one with some other source parameters to get a better fitting.

We have fitted the limb-darkening and accretion disk model light curves with that of the Gaussian source of different radii. The half-brightness radius varied from $R_{1/2} = 0.2R_{\rm E}$ to $R_{1/2} = 0.24R_{\rm E}$; here, $p = 3/2$ and $q = 1$.

As we can see from Fig. 6 and Table 4, the Gaussian source cannot reproduce all the models, though the fitting results are rather good for the class of compact models. For example, the LD model can be replaced by the Gaussian model with the other source size. The relative differences between models in Fig. 6 and Table 4

T a b l e 3. Differences between source's models with the same $R_{\rm rms} = 0.21R_{\rm E}$ parameter in simple caustic crossing events; here, $p = 3$, $q = 1$

i-th model	j-th model	η
AD1	Gaussian	0.12 ± 0.04
LD	Gaussian	0.03 ± 0.01
PL	Gaussian	0.05 ± 0.012
AD1	LD	0.14 ± 0.05
AD1	Power-law	0.08 ± 0.03
LD	PL	0.08 ± 0.02

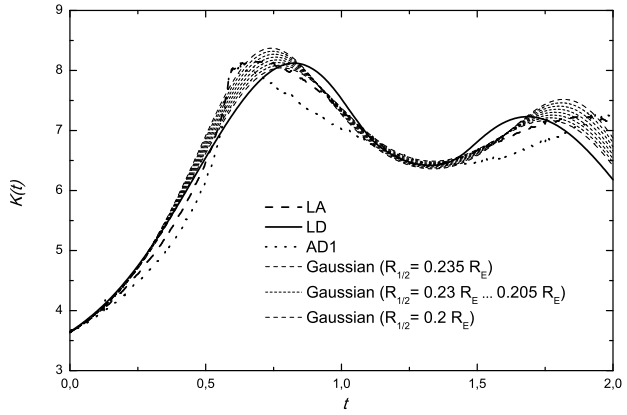


Fig. 5. Light curves of the LD, AD1 and AL models are fitted with a Gaussian source of different sizes from $R_{1/2} = 0.2R_{\rm E}$ to $R_{1/2} = 0.24R_{\rm E}$ with step $\delta R_{1/2} = 0.001R_{\rm E}$. These light curves correspond to the magnification pattern of Fig. 3

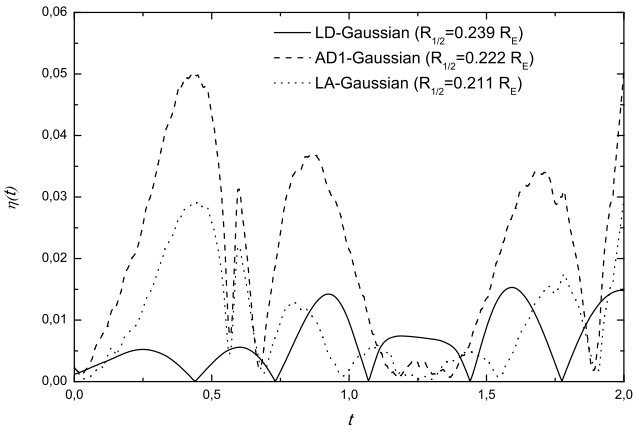


Fig. 6. Relative differences between the Gaussian, LD, AD1, and LA models for best fitted curves

show that it is possible to fit a considerable part of the whole curve with different source models on the accuracy level which is comparable to that of modern photometric observations.

4. Approximation Methods

4.1. Statement of the problem

The study of a caustic crossing event is closely related to the investigation of the lens equation solutions. This equation near a fold can be expanded in powers of local coordinates; in the lowest orders of this expansion, the caustic is represented by a straight line; so, this approximation is often referred as a "linear caustic approximation". In this approximation, the point source flux amplification is given by a simple formula (5) including the distance to the caustic and two fitting parameters. In the most known cases, the linear caustic approximation is sufficient to fit the observed light curves during HAEs at the modern accuracy of flux measurements. At the same time, the consideration of "post-linear" terms is sometimes necessary to explain the present observational data. The need for a modification of this formula – e.g., by taking the caustic curvature into account – is being discussed for a long time [9, 30, 31]. The corrections to the amplification coefficient in the case of the macrolensing were the subject of investigations dealing with the problem of "anomalous flux ratios" [32]. A modification of the post-linear approximation allows one to improve the quality of the fitting of the HAE light curve of the image C in the GLS "Einstein Cross" [33, 34]. One may hope for that an improvement of the photometric accuracy of GLS observations will make it possible to obtain additional parameters of the lens mapping connected with the mass distribution in the lensing galaxy. Below, we study some points of an approximate solution of the lens equation near the fold caustic which probably is crossed by the source in many HAEs.

T a b l e 4. Differences between models for fitted curves

i-th model	j-th model	η
AD	Gaussian ($R_{1/2} = 0.2$)	0.07 ± 0.006
LD	Gaussian ($R_{1/2} = 0.24$)	0.026 ± 0.002
LA	Gaussian ($R_{1/2} = 0.2$)	0.034 ± 0.006

The standard consideration of the caustic crossing events deals with the Taylor expansion of the potential near some point of the critical curve in the image plane. Let this point be the coordinate origin in an appropriate coordinate system, and let this point map onto the coordinate origin of the source plane. Further, we rotate the coordinate systems in both planes so that the abscissa axis on the source plane is tangent to the caustic at the origin, the quantity $|y_2|$ defines locally the distance to the caustic, and y_1 defines a displacement along the tangent. For the harmonic potential, we can write the corresponding lens equation as

$$y_1 = 2x_1 + a\left(x_1^2 - x_2^2\right) + 2bx_1x_2 + c\left(x_1^3 - 3x_1x_2^2\right) - \\ -d\left(x_2^3 - 3x_2x_1^2\right) + gx_2^4 + ...,$$

$$y_2 = \ b\left(x_1^2 - x_2^2\right) - 2ax_1x_2 + d\left(x_1^3 - 3x_1x_2^2\right) + \\ +c\left(x_2^3 - 3x_2x_1^2\right) + fx_2^4 + ..., \qquad (16)$$

where a, b, c, d, g, and f are expansion coefficients. If the y_2 axis is directed toward the convexity of the caustic, then $b < 0$ (at fold points, $b \neq 0$).

We now proceed to the derivation of approximate solutions of Eqs. (16). To do this, we present two different methods [33]. The first method deals with analytic expansions in powers of a small parameter. However, it results in nonanalytic functions of coordinates leading to nonintegrable terms in the amplification coefficient. The second method does not lead to such problems, though it uses a somewhat more complicated representation of the solution of the lens equation containing square roots of analytic functions. The methods agree with each other in a common domain of validity; moreover, we use the second method to justify some expressions in the amplification formulas in terms of distributions to validate the applications to extended source models. A more detailed presentation may be found in [33].

First, we suppose that the source and the caustic lie on different sides from the y_1 axis. Then, $y_2 > 0$, and we substitute

$$y_i = t^2 \tilde{y}_i, \quad x_1 = t^2 \tilde{x}_1, \quad x_2 = t\tilde{x}_2, \tag{17}$$

where $i = 1, 2$, and t can be considered as a parameter of vicinity to the caustic. This is a formal substitution that makes easier the operations with different orders of the expansion. After calculations, we put $t = 1$ and thus return to the initial variables y_i. However, if we put $\tilde{y}_i$ to be constant with varying t, then this substitution allows us to study a local behavior of critical image trajectories; $t = 0$ corresponds to crossing the caustic by a point source, when two critical images appear. As was shown in [33], this allows one to look for solutions of Eqs. (16), by using the expansions of $\tilde{x}_i$ in powers of t:

$$\tilde{x}_1 = \tilde{x}_{10} + \tilde{x}_{11} t + \tilde{x}_{12} t^2 + ...,$$

$$\tilde{x}_2 = \tilde{x}_{20} + \tilde{x}_{21} t + \tilde{x}_{22} t^2 + ... \tag{18}$$

It should be stressed that the analyticity in t does not mean that the coefficients of expansions (18) will be analytic functions of coordinates $\tilde{y}_i$ in the source plane (see below).

In terms of the new variables (17), system (16) takes the form (up to the terms $\sim t^2$)

$$\tilde{y}_1 = 2\tilde{x}_1 - a\tilde{x}_2^2 + t(2b\tilde{x}_1\tilde{x}_2 - d\tilde{x}_2^3) +$$

$$+ t^2(a\tilde{x}_1^2 - 3c\tilde{x}_1\tilde{x}_2^2 + g\tilde{x}_2^4),$$

$$\tilde{y}_2 = -b\tilde{x}_2^2 + t(-2a\tilde{x}_1\tilde{x}_2 + c\tilde{x}_2^3) +$$

$$+ t^2(b\tilde{x}_1^2 - 3d\tilde{x}_1\tilde{x}_2^2 + f\tilde{x}_2^4). \tag{19}$$

The substitution of expansions (18) into (19) allows us to determine all coefficients successively. For example, for the zero-order terms, we have

$$\tilde{x}_{10} = \frac{1}{2}\left(\tilde{y}_1 - \frac{a}{b}\tilde{y}_2\right), \quad \tilde{x}_{20} = \varepsilon\sqrt{\tilde{y}_2/\left|b\right|}\,, \tag{20}$$

where $\varepsilon = \pm 1$ determines two different critical solutions. This approximation yields the well-known formula for the amplification (5).

The first-order approximation terms have been derived in [32, 35]. In microlensing observations, two critical images cannot be resolved, so we need the total amplification coefficient of two critical images. However, the contributions of the order of $\sim t$ appear to be cancelled in calculations of the total amplification. Therefore, to obtain a nontrivial correction to the zero-order amplification, higher order approximations should be involved. These corrections have been derived in [33, 34]. Note that the corresponding second-order terms contain expressions nonanalytic in $\tilde{y}_2$. Though the second-order corrections are expected to be small, they appear to be noticeable in some cases even in the analysis of the available data on light curves in the Q2237+0305 GLS.

4.2. Method 2

The other approach to the construction of approximate solutions of the lens equation in a vicinity of the fold is described in [33]. This allows us to present the critical solutions of system (19) in the following form:

$$\tilde{x}_1 = p + tr\varepsilon\sqrt{w},$$

$$\tilde{x}_2 = t\bar{s} + \varepsilon\sqrt{w}, \quad \varepsilon = \pm 1. \tag{21}$$

After the substitution of Eqs. (21) in the lens equation, the terms containing integer and half-integer powers of w can be separated [33]. After some algebra, this yields a system that is convenient for an iterative procedure resulting in analytic expansions for the functions $p, r, \bar{s}, w$ both in powers of t and $\tilde{y}_i$ at every step of iteration [33]. In [33], such a solution was obtained up to the terms $\sim t^2$. If we expand $\sqrt{w}$ in powers of t, then we immediately have the solution in the form (18).

4.3. Amplification of a point source

The solutions of the lens equation are then used to derive the Jacobians of the lens mapping (for both images near the critical curve). According to (2), the value of J^{-1} yields the amplification of individual images. As we pointed out above, we need the total amplification of two critical images (the sum of two amplifications of the separate critical images). In the second-order approximation (using the expansion up to the terms t^2), this is

$$K_{\rm cr} = \frac{1}{2}\frac{\Theta\left(y_2\right)}{\sqrt{|b|\,y_2}}\left[1 + Py_2 + Qy_1 - \frac{\kappa}{4}\frac{y_1^2}{y_2}\right], \qquad (22)$$

where the constants P and Q are expressed via the Taylor expansion coefficients from Eq.(1), and

$$\kappa = \frac{a^2+b^2}{2\,|b|}\,;$$

$\Theta(y_2)$ is the Heaviside step function. Note that κ is the caustic curvature at the origin which enters explicitly into the amplification formula. The parameters P and Q are independent; the explicit formulae for them can be found in [33, 34]. However, this is not needed when we use Eq.(22) for fitting the observational data, because these constants are whatever considered as free fitting parameters.

Formula (22) yields an effective approximation for the point source amplification near the coordinate origin provided that $y_2 > 0$, and y_2/y_1^2 is not too small (see the term containing κ). For a fixed source position, this can be satisfied always by an appropriate choice of the coordinate origin, so that the source will be situated almost on a normal to the tangent to the caustic.

If the source is on the caustic tangent or in the region between the caustic and the tangent, then formula (22) does not give a good approximation to the point source amplification. Nevertheless, in the case of an extended source, we will show that result (22) can be used to obtain approximations to the amplification of this source even as it intersects the caustic. However, to do this, we need to redefine correctly the convolution of (22) with a brightness distribution.

5. Amplification of Extended Sources

5.1. Transition to extended sources

We now present the results of studies of the point source amplification within extended source models. Let $I(\mathbf{y})$ be a surface brightness distribution of an extended source. If the source center is located at the point $\mathbf{Y} = (Y_1, Y_2)$ in the source plane, then the total microlensed flux from the source is given by (4).

Formula (22) contains the nonintegrable term $\sim \Theta(y_2)(y_2)^{-3/2}$. Therefore, the question arises of how formula (22) can be used in the situation where the extended source intersects a caustic and some part of the source is in the zone between the tangent and the caustic. In view of Section 4, it is evident that the mentioned term is a result of the asymptotic expansion of the root $\sqrt{y_2 + \kappa y_1^2 t^2/2 + ...}$ in the approximate solution (21). The direct usage of a solution in the form (21) for the calculation of the Jacobians of the lens mapping and then for the derivation of amplifications does not lead to any divergences, and any nonintegrable terms in $K_{\rm cr}$ do not arise. Nevertheless, it is convenient to have a representation of $K_{\rm cr}$ in the form of an expansion in powers of a small parameter. Such an expansion can be carried out correctly after the substitution of $K_{\rm cr}$ into integral (4). On this way, starting from (21), it is easy to show that, to define $K_{\rm cr}$ correctly, one must replace the term $\Theta(y_2)(y_2)^{-3/2}$ in (22) by the distribution (generalized function) $(y_2)_+^{-3/2}$ [36]. We recall that the distribution $y_+^{-3/2}$ of the variable y is defined by the expression

$$\int y_+^{-3/2} f(y)dy = 2\int\limits_0^\infty y^{-1/2}\frac{\partial f(y)}{\partial y}dy$$

for any test function $f(y)$.

After this redefinition, we have

$$K_{\rm cr} = \frac{\Theta\left(y_2\right)}{2\sqrt{|b|\,y_2}}\left[1 + Py_2 + Qy_1\right] - \frac{\kappa}{8\sqrt{|b|}}y_1^2(y_2)_+^{-3/2}. \qquad (23)$$

This formula can be used to correctly derive an approximate amplification of a sufficiently smooth extended source including the case where the source crosses the caustic.

5.2. Gaussian source

Formula (23) has been used [33] to derive the amplification of a Gaussian source with the brightness distribution (8), the limb-darkening source, and the power-law source (see the next subsections).

Further, we use the dimensionless coordinates $s = Y_1/R$, $h = Y_2/R$ of the source center and the functions

$$I_k\left(h\right) = \int\limits_0^\infty u^{k-1/2}\exp\left(-u^2 + 2uh\right)du =$$

$$= \frac{1}{2}\sum_{n=0}^{\infty}\frac{\Gamma\left(\frac{1}{4}+\frac{k+n}{2}\right)}{n!}(2h)^n. \quad (24)$$

These functions can be expressed in terms of the confluent hypergeometric function ${}_1F_1$ or the parabolic cylinder function D:

$$I_k(h) = 2^{-\left(\frac{k}{2}+\frac{1}{4}\right)}\Gamma\left(k+\frac{1}{2}\right)e^{\frac{h^2}{2}}D_{-\left(k+\frac{1}{2}\right)}\left(-\sqrt{2}h\right). \quad (25)$$

The substitution of (23) and (8) in (4) yields

$$K_G(s,h) = \frac{1}{2\sqrt{\pi\,|b|\,R}}\Big\{\Phi_0(h) + \\ +R\left[P\Phi_1(h) - \frac{\kappa}{2}\Phi_2(h) + Qs\Phi_0(h) - \kappa s^2\Phi_2(h)\right]\Big\}. \quad (26)$$

Here,

$$\Phi_0(h) = I_0(h)\exp\left(-h^2\right),$$

$$\Phi_1(h) = I_1(h)\exp\left(-h^2\right),$$

$$\Phi_2(h) = \left[hI_0(h) - I_1(h)\right]\exp\left(-h^2\right).$$

Note that the main term of (26) which corresponds to the linear caustic approximation was first obtained in work [37].

5.3. Limb-darkening source

Analogous considerations allow us to obtain formulas for the amplification of extended sources for the limb-darkening and power-law brightness profiles; the results are represented analytically in terms of the hypergeometric function ${}_2F_1$ [38].

Denote

$$\mathrm{X}_{k,q}(h) = \frac{\Gamma(q+2)}{\Gamma\left(q+\frac{3}{2}\right)}\int_0^{\infty} y^{k-\frac{1}{2}}\,\Xi(y-h;q+1/2)\,dy,$$

$k = 1, 2$. We have

$$X_{k,q}(h) = 2^{q+\frac{1}{2}}(1+h)^{q+k+1}\frac{\Gamma(q+2)\Gamma(k+\frac{1}{2})}{\Gamma(q+k+2)}\times \\ \times\ {}_2F_1\left(-q-\frac{1}{2}, q+\frac{3}{2}; q+k+2; \frac{1+h}{2}\right)$$

for $-1 < h < 1$ and

$$\mathrm{X}_{k,q}(h) = \\ = \sqrt{\pi}\,(h+1)^{k-\frac{1}{2}}\,{}_2F_1\left(q+\frac{3}{2}, \frac{1}{2}-k; 2q+3; \frac{2}{h+1}\right)$$

for $h > 1$.

For $k = -1$, we define

$$\mathrm{X}_{-1,q}(h) = 4(q+1)\left(h\mathrm{X}_{0,q-1} - \mathrm{X}_{1,q-1}\right).$$

Then, in case of the model with limb darkening (9), the critical images disappear when the source lies on the outer side of the caustic (i.e., for $h < -1$). The amplification due to critical images takes the form

$$K_{\mathrm{LD}}(s,h) = \frac{1}{2\sqrt{\pi|b|R}}\Big\{\mathrm{X}_{0,q}(h) + R\Big[P\mathrm{X}_{1,q}(h) - \\ -\frac{\kappa}{8(q+2)}\mathrm{X}_{-1,q+1}(h) + Q\,s\,\mathrm{X}_{0,q}(h) - \frac{\kappa}{4}\,s^2\mathrm{X}_{-1,q}(h)\Big]\Big\}.$$

5.4. Amplification for a power-law source

The result for the amplification involves integrals:

$$\Psi_{k,p}(h) = \frac{\Gamma\left(p-\frac{1}{2}\right)}{\Gamma(p-1)}\int_0^{\infty}\frac{y^{k-\frac{1}{2}}dy}{\left(1+(y-h)^2\right)^{p-1/2}} = \\ = \frac{\Gamma\left(p-\frac{1}{2}\right)}{\Gamma(p-1)}B\left(k+\frac{1}{2}, 2p-k-\frac{3}{2}\right)(1+h^2)^{k/2+3/4-p}\times \\ \times\ {}_2F_1\left(k+\frac{1}{2}, 2p-k-\frac{3}{2}; p; \frac{1}{2}\left(1+\frac{h}{\sqrt{1+h^2}}\right)\right)$$

for $k = 0, 1$, $B(x,y)$ being the Beta-function.

We extend this to $k = -1$ in view of the definition of $(y)_+^{-3/2}$. So, we have

$$\Psi_{-1,p}(h) = 4(p-1)[h\Psi_{0,p+1}(h) - \Psi_{1,p+1}(h)].$$

Now, the amplification due to critical images takes the form

$$K_{\mathrm{PL}}(s,h) = \frac{1}{2\sqrt{\pi|b|R}}\Big\{\Psi_{0,p}(h) + R\Big[P\Psi_{1,p}(h) - \\ -\frac{\kappa}{8(p-2)}\Psi_{-1,p-1}(h) + Q\,s\,\Psi_{0,p}(h) - \frac{\kappa}{4}\,s^2\Psi_{-1,p}(h)\Big]\Big\}.$$

The zeroth approximation to this formula has been derived in [9].

6. Discussion

Prior to sum up the results of this paper, we must stress that the consideration of HAEs without some additional information may only provide a very uncertain, on order-of-magnitude level, and even ambiguous information about the source parameters. For example, one may expect that, by adding a sufficient number of small microlenses, it is possible to reproduce fine features of a light curve during a HAE and to fit the light curve of any compact source. The introduction of planetary mass objects in the lensing galaxy (which is quite reasonable, see, e.g., [39–42]) yields a fine caustic mesh, which, in turn, can give rise to fine features of light curves during a HAE similar to those due to any given brightness distribution over the source. Therefore, we point out the assumptions and the class of models involved, which is necessary for a reasonable formulation of the problem.

The simulations of the present paper use the GLS parameters similar to those of Q2237+030 [26, 42]. We consider the equal mass microlensing system; we do not consider any mass distributions and/or populations of small (planetary) masses. Next, we consider the most simple source models without effects of ellipticity, *etc.* Nevertheless, we see that, even under these rather severe restrictions, there is an ambiguity in the determination of the source model from the observations of HAEs. The limb-darkening source can be successively fitted with the Gaussian source model (with the other $R_{1/2}$) on 1-2% accuracy level. This confirms the conclusions of Mortonson *et al.* [17] (see also [43]) that the surface brightness profile has little effect on microlensing. What can be determined within the modern accuracy is the source size; one can also distinguish either we deal with a compact source or not (i.e., with a steep decrease of the brightness for large radii).

The investigation of the source structure from HAEs is closely related to the solution of the lens equation in the caustic region. There are also different approaches to this problem under different restrictions. In this paper, we confined ourselves to the case of the fold caustic. We outlined two methods that enable us to obtain the critical solutions of the gravitational lens equation near a fold with any desired accuracy [33, 34]. In order to obtain nontrivial corrections to $K_{\rm cr}$ obtained in the linear caustic approximation, the higher orders of the expansion of the lens equation must be taken into account, as compared to works [32, 35]. The modified formula for $K_{\rm cr}$ contains three extra parameters. This is applied to the Gaussian, power-law, and limb darkening models of an extended source. The fitting of the light curve of GLS Q2237+0305C using these modified relations shows [33, 34] that some of these corrections can be statistically significant even at the present accuracy level. This means that if we are looking for some fine effects in HAEs due to the source size, a consistent treatment must involve sometimes the higher-order corrections to solutions of the lens equation.

This work has been supported in part by the "Cosmomicrophysics" program of the National Academy of Sciences of Ukraine. We are grateful to the staff of the Computer Center of National Technical University of Ukraine "Kyiv Polytechnic Institute", where a considerable part of our simulations has been performed.

1. P. Schneider, J. Ehlers, and E.E. Falko, *Gravitational Lenses* (Springer, New York, 1992).
2. J. Wambsganss, *Gravitational Lensing: Strong, Weak, and Micro*, edited by G. Meylan, P. North, and P. Jetzer (Springer, Berlin, 2006), p. 453.
3. B. Grieger, R. Kayser, and S. Refsdal, A&A **194**, 54 (1988).
4. J. Huchra, V. Gorenstein, S. Kent, I. Shapiro, G. Smith, E. Horine, and R. Perley, AJ **90**, 691 (1985).
5. D. Alcalde, E. Mediavilla, O. Moreau, J.A. Munoz, C. Libbrecht *et al.*, ApJ **572**, 729 (2002).
6. A. Udalski *et al.*, Acta Astron. **56**, 293 (2006).
7. P.R. Wozńiak, C. Alard, A. Udalski, M. Szymański, M. Kubiak, G. Pietrzyński, and K. Zebruń, ApJ **529**, 88 (2000).
8. M.B. Bogdanov and A.M. Cherepashchuk, Astron. Repts. **46**, 626 (2002).
9. V.N. Shalyapin, Astron. Lett. **27**, 150 (2001).
10. V.N. Shalyapin, L.J. Goicoechea, D. Alcalde, E. Mediavilla, J.A. Muñoz, and R. Gil-Merino, ApJ **579**, 127 (2002).
11. J.S. Wyithe, R.L. Webster, and E.L. Turner, MNRAS **309**, 261 (1999).
12. J.S. Wyithe, R.L. Webster, and E.L. Turner, MNRAS **318**, 762 (2000).
13. J.S. Wyithe, R.L. Webster, E.L. Turner, and D.J. Mortlock, MNRAS **315**, 62 (2000).
14. A. Yonehara, AJ **548**, 127 (2001).
15. R. Gil-Merino, J. Gonzalez-Cadelo, L.J. Goicoechea, V.N. Shalyapin, and G.F. Lewis, MNRAS **371**, 1478 (2006).
16. L.J. Goicoechea, D. Alcalde, E. Mediavilla, and J.A. Muñoz, A& A **397**, 517 (2003).
17. M.J. Mortonson, P.L. Schechter, and J. Wambsganss, ApJ **628**, 594 (2005).

18. C.S. Kochanek, ApJ **605**, 58 (2004).
19. T. Anguita, R.W. Schmidt, E.L. Turner, J. Wambsganss, R.L. Webster, K.A. Loomis, D. Long, and R. MacMillan, A&A **480**, 327 (2008).
20. S. Poindexter and C.S. Kochanek, ApJ **712**, 658 (2010).
21. S. Poindexter and C.S. Kochanek, ApJ **712**, 668 (2010).
22. S. Poindexter, N. Morgan, and C.S. Kochanek, ApJ **673**, 34 (2008).
23. V.G. Vakulik, R.E. Schild, G.V. Smirnov, V.N. Dudinov, and V.S. Tsvetkova, MNRAS **382**, 819 (2007).
24. M. Dominik, MNRAS **353**, 69 (2004).
25. N.I. Shakura and R.A. Sunyaev, Astron. Astrophys. **24**, 337 (1973).
26. R. Schmidt, R.L. Webster, and F.G. Lewis, MNRAS **295**, 488 (1998).
27. X. Dai, E. Agol, M.W. Bautz, and G.P. Garmire, ApJ **589**, 100 (2003).
28. E.V. Fedorova, V.I. Zhdanov, C. Vignali, and G.G.C. Palumbo, A&A **490**, 989 (2008).
29. V. Vakulik, R. Schild, V. Dudinov, S. Nuritdinov, V. Tsvetkova, O. Burkhonov, and T. Akhunov, A&A **447**, 905 (2006).
30. C.J. Fluke and R.L. Webster, MNRAS **302**, 68 (1999).
31. A.B. Congdon, C.R. Keeton, and C.E. Nordgren, MNRAS **389**, 398, (2008).
32. C.R. Keeton, B.S. Gaudi, and A.O. Petters, ApJ **635**, 35 (2005).
33. A.N. Alexandrov and V.I. Zhdanov, e-print arXiv:1006.5903 (2010).
34. A.N Alexandrov, V.I Zhdanov, and E.V. Fedorova, Astron. Lett. **36**, 329 (2010).
35. A.N Alexandrov, V.I Zhdanov, and E.V. Fedorova, Visn. Kyiv. Univ., Astron. **39-40**, 52 (2003).
36. I.M. Gel'fand and G.E. Shilov, *Generalized Functions, Vol. 1* (Academic Press, New York, 1964).
37. P. Schneider and A. Weiss, A&A **171**, 49 (1987).
38. H. Bateman and A. Erdélyi, *Higher Transcendental Functions, Vol. 1* (McGraw-Hill, New York, 1953).
39. M. Jaroszynski, B. Paczynski, AA **52**, 361 (2002).
40. S. Mao and B. Paczynski, ApJ **374**, 37 (1991).
41. Y. Tsapras, K. Horne, S. Kane, and K. Carson, MNRAS **343**, 1131 (2003).
42. J.S.B. Wyithe and E.L. Turner, MNRAS **320**, 21 (2001).
43. A.B. Congdon, C.R. Keeton, and S.J. Osmer, MNRAS **376**, 263 (2007).

Received 30.01.11

ЕФЕКТИ ПЕРЕТИНУ КАУСТИКИ І МОДЕЛІ ДЖЕРЕЛА У ГРАВІТАЦІЙНО-ЛІНЗОВИХ СИСТЕМАХ

О.М. Александров, В.М. Слюсар, В.І. Жданов

Р е з ю м е

Події з великим підсиленням (ПВП) є звичайним явищем у позагалактичних гравітаційно-лінзових системах (ГЛС), де спостерігають декілька зображень віддаленого квазара на фоні галактики, що знаходиться на передньому плані. Протягом ПВП відбувається значне збільшення яскравості в одному із зображень квазара. Грігер, Кайзер та Рефсдал запропонували використовувати ПВП для вивчення центральних областей квазара в ГЛС. У цій статті досліджуємо пов'язані з цим питання, що стосуються ідентифікації різних типів джерела на базі спостережень ПВП. Ми порівнюємо результати числових моделювань кривих блиску для того, щоб оцінити можливість відрізнити моделі джерела в ГЛС. Запропоновано наближені схеми для розв'язання рівняння лінзи в околі каустики – складки. Результати використано для отримання коефіцієнтів підсилення, що враховують поправки високого порядку для моделей гаусівського і степеневого джерела, а також джерела з потемнінням до краю.